J Nanostruct 16(1): 744-755, Winter 2026

RESEARCH PAPER

Effect of Sintering on the Microstructure and Mechanical Properties of Ti–Mo Alloys: A Promising Approach for Biomedical Applications

Abdulmalek Sultan Merie *, Adnan M. Khalid

Department of Physics, College of Science, Tikrit University, Tikrit, Iraq

ARTICLE INFO

Article History:
Received 11 August 2025
Accepted 24 December 2025
Published 01 January 2026

Keywords:
Biomedical applications
Hardness
Microstructure
Sintering
Ti–Mo alloys

ABSTRACT

Aluminum (Al) and vanadium (V) are known to exhibit cytotoxic effects; nevertheless, titanium-based alloys have been widely employed in biomedical implants. Recent research has therefore focused on the development of Al- and V-free titanium alloys incorporating non-cytotoxic β-stabilizing elements such as molybdenum (Mo). In this study, the influence of Mo content on the structural, microstructural, and mechanical properties of Ti–xMo alloys (x = 25, 30, and 35 wt.%) was systematically investigated. The prepared nano-powders were characterized before and after sintering at 1150 °C using X-ray diffraction (XRD), field-emission scanning electron microscopy (FE-SEM), energy-dispersive X-ray spectroscopy (EDX), and Vickers micro-hardness testing. FE-SEM analysis revealed distinct Ti and Mo nanoparticle morphologies and sintering-induced particle growth with spherical features governed by Mo content and enhanced atomic diffusion. A reduction in particle size at 35 wt.% Mo was attributed to solubility limits and saturation effects within the titanium lattice. XRD and EDX analyses verified phase evolution without the presence of impurities and revealed partial oxide reduction after sintering. The titanium alloy containing 35 wt.% molybdenum exhibited the highest hardness value of 375 HV, representing a significant improvement compared to pure nanocrystal line titanium, which recorded a hardness of 170 HV. These results confirm the close relationship between structure and properties, making Titanium-Molybdenum alloys highly promising materials for use in advanced biomedical implant applications.

How to cite this article
Merie A., Khalid A. Effect of Sintering on the Microstructure and Mechanical Properties of Ti–Mo Alloys: A Promising Approach for Biomedical Applications. J Nanostruct, 2026; 16(1):744-755. DOI: 10.22052/JNS.2026.01.067

INTRODUCTION

Titanium and titanium alloys are used more and more as opposed to the traditional metallic biomaterials, including stainless steel, cobalt-chromium alloys, among others, mostly because they are highly biocompatible. One of the primary characteristics of titanium alloys is their low density of about 4.5 g/cm^3 which is almost one-half the density of iron- and cobalt-based alloys [1]. Moreover, the alloys show exceptional resistance to in vivo corrosion, such as, pitting and crevice corrosion [2]. Therefore, biological reactivity is reduced due to the high chemical stability of titanium, which encourages the process of tissue

* *Corresponding Author Email: Abdulmalek.sultan@st.tu.edu.iq*

healing and increases the useful duration of implants many times [3, 4]. Besides this, titanium is also getting cheaper as its demand has increased in various industries including aerospace, sports and recreation [5, 6]. Examples of the most popular titanium alloys in the work of implants are Commercially Pure Titanium (CP-Ti) and Ti-6Al-4V ELI which is an (alpha +beta) alloy that is also common in the aerospace sector. Nonetheless, each of the materials has certain restrictions: CP-Ti is not strong enough mechanically, and Ti-6Al-4V ELI has alloying elements that can be potentially dangerous to health [7]. Depending on the crystal structure, titanium alloys are typically divided into three major types: α-alloy, β-alloy and (α + β)-alloy. The alpha and beta alloys have a single-phase microstructure and the (α + β) alloys have a dual phase structure. [8, 9]. Added 10-15% β-stabilizing elements play a major role in making b phase metastable at ambient temperatures [9], and thus allow fine control of the b-phase volume fraction. [10, 11]. With respect to biomechanical considerations, medical implants must demonstrate appropriate mechanical strength to support the physiological forces created by the musculoskeletal forces. Thus, mechanical characteristics of any biomaterial device must be adjusted to the requirements of particular functional needs of the host tissues and bone. [12]. Moreover, the mechanical properties of these materials are easily increased with the help of a variety of processing methods that have long been established. Consequently, orthopedics and medical field in general have been exposed to the large scale application of titanium and its alloys in clinical practice. [13, 14]. The most popular and commonly used orthopedic implant material, still in use today, is Commercially Pure Titanium (cp-Ti), usually with an a-microstructure, and some (α + β)-based alloys, including Ti-Al-Fe and Ti-Al-Nb. This choice is based on its superior qualities, which are the excellent biocompatibility, high corrosion resistance, and incredible amount of strength to weight ratio. [15]. Although the commonly used Ti alloys are prevalent, they have significant drawbacks. Since Niinomi et al and Chui et al have pointed out that These materials have a Youngs modulus that is significantly higher than that of human bone, biomechanical incompatibility would occur. The difference in this stiffness results in a stress-shielding effect, i.e. the load that is supposed to go on the bone is transferred to the implant and may cause bone resorption and premature implant failure. [18]. Moreover, such alloys as Ti-Al-Fe and Ti-Al-V have biological issues because they can emit cytotoxic ions, i.e. aluminum (Al) and vanadium (V) [19]. Prolonged exposure of these ions in vivo has been linked to neurotoxicity such as a relationship to Alzheimer disease. Consequently, the research has shifted towards the development of low-modulus titanium alloys composed purely of elements that are biocompatible including Mo, Nb, Zr, Ta, and Sn [20]. Campos-Quiros et al. found that Ti-Nb-Zr, Ti-Mo-Zr-Fe, and Ti-Mo systems have a promising future [21]. Structurally, β-type alloys are favored for their bone-mimicking mechanical properties. For instance, Xu et al. [22] utilized X-ray diffraction (XRD) to confirm a single β -phase structure in Ti-35Zr-28Nb. Similarly, Phasha and Raganya [23] determined that Mo contents of 17 and 20 wt.% in binary Ti–Mo alloys differ optimal properties for biomedical use. Li et al. [24] further demonstrated that Ti–10Mo–(3, 7, 10)Nb alloys offer a superior balance of high strength and low elastic modulus, attributed to the formation of a dominant equiaxed β-phase promoted by Mo and Nb additions [25] investigated binary Ti–Mo alloys with Mo contents ranging from 6–20 wt.% and reported microhardness values (270–340 HV) significantly higher than those of commercially pure Ti (160 HV). Among the alloys, the α″-phase Ti–7.5Mo exhibited the lowest hardness (263 HV), whereas β-phase alloys, particularly those containing 10 and 12.5 wt.% Mo, showed the highest hardness. Recently, extensive investigations have focused on the impact of Molybdenum (Mo) content on the physicochemical properties of binary Ti–xMo alloys. In the context of ternary systems, biomedical-grade Ti–Mo–O alloys characterized by a dual-phase (α+β) microstructure demonstrate a superior mechanical synergy. Specifically, these alloys exhibit an exceptional balance between tensile strength and ductility, achieving tensile strengths exceeding 1150 MPa while maintaining high total strain values. Mechanical performance is governed by both phase fractions and solid-solution strengthening of the α phase by oxygen and the β phase by molybdenum. Therefore, optimizing α/β ratios and controlling Mo and O concentrations are essential to achieve high strength, hardness, and ductility [26,27,28]. Several studies have applied powder metallurgy, particularly high-energy ball milling, to produce

β-type titanium alloys with enhanced mechanical properties optimized for biomedical applications [29,30,31]. Therefore, the aim of this study is to develop β-type titanium-based alloys with novel chemical compositions and to investigate the effect of the milling process on the structural evolution and mechanical behavior of the Ti–xMo system (x = 25, 30, 35 wt.%), with a view toward optimizing these alloys as a promising option for biomedical applications.

MATERIALS AND METHODS

Samples preparation

Titanium and molybdenum nanoparticles with an average particle size of 60–80 nm and purities of 99.9% and 99.7%, respectively, supplied by Skyspring Nanomaterials, Inc. (USA), were used as starting materials. The samples were prepared using commercially available pure elemental nano-powders. Stoichiometric amounts of the starting elemental powders were weighed using a precision balance to prepare Ti-xMo alloys (x = 20, 25, 30$ wt.%), which were subsequently synthesized via high-energy mechanical alloying (MA) in a planetary ball mill (Fritsch Pulverisette P7) under an argon atmosphere to prevent oxidation. The milling process utilized an 80 ml agate vial and 10 mm agate balls with a ball-to-powder weight ratio of 10:1, operating at a rotational speed of 300 rpm for a total duration of 18h, to mitigate thermal accumulation, a cyclic protocol of 15 min milling followed by a 5 min cooling interval was employed. Following synthesis, the pre-alloyed powders were consolidated via a standard powder metallurgy route, where they were loaded into a rigid steel die and uniaxially compressed at]400 MPa using a manual hydraulic press with a holding time of 5 min to yield cylindrical green compacts (2 cm diameter, 5 mm thickness). Finally, the green compacts were sintered in a vacuum furnace (Nabertherm GmbH, Germany) by heating at a rate of 10 °C/min to 1150 °C for a dwell time of 2 h under an applied pressure of 12 MPa, followed by gradual furnace cooling to room temperature, as illustrated in the thermal and pressure cycles in Fig. 1.

Materials characterizations

Structural characterizations

X-ray diffraction (XRD) analysis was conducted using a Siemens D5000 diffractometer with CuKα radiation (λ = 1.541 Å), operated at 40 kV and 40 mA. Diffraction patterns were recorded with a step size of 0.02° and a counting time of 2 s per

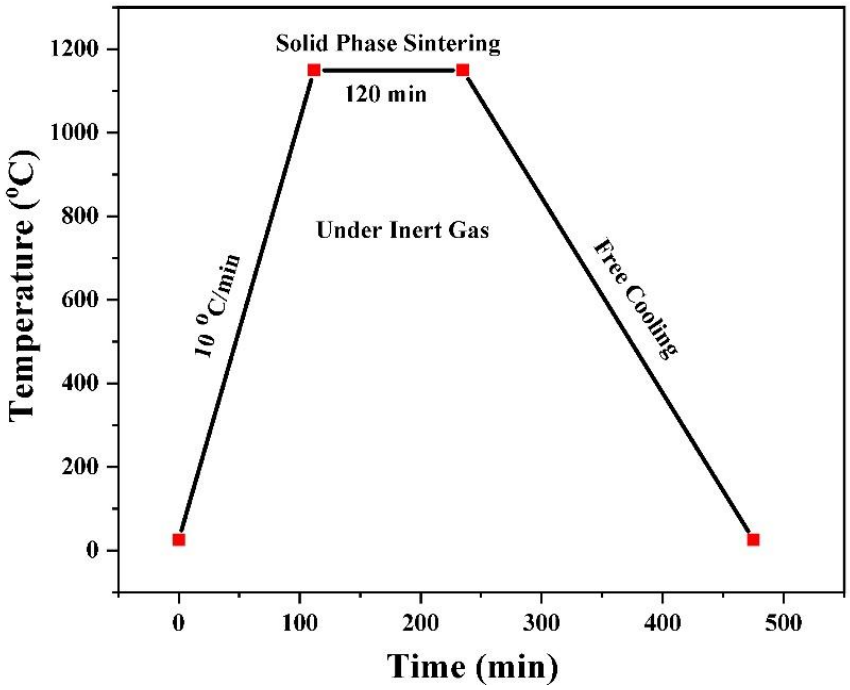

Fig. 1. Sintering program applied to the samples prepared in this study.

step. The microstructure and morphology of the milled and consolidated samples were examined using scanning electron microscopy (SEM, FE-Quanta 250, USA), while energy-dispersive X-ray spectroscopy (EDS) was employed for quantitative elemental analysis.

Mechanical characterizations

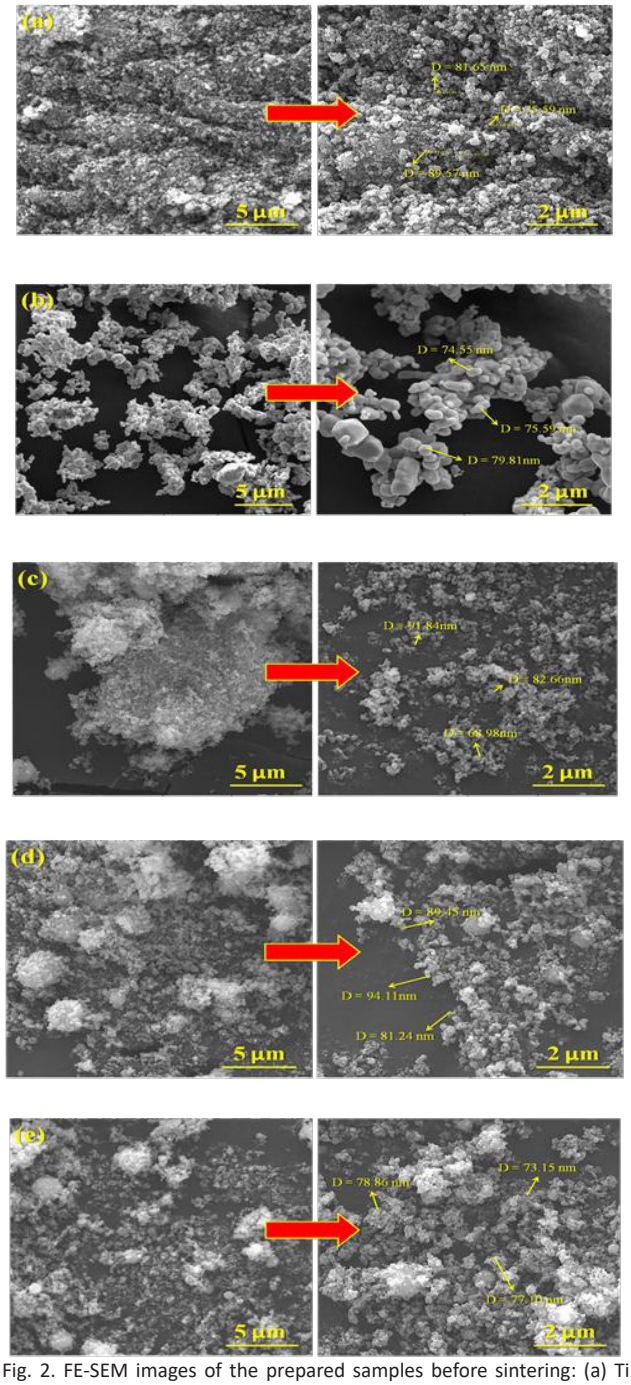

Fig. 2. FE-SEM images of the prepared samples before sintering: (a) Ti nanoparticles, (b) Mo nanoparticles, (c) Ti–25Mo, (d) Ti–30Mo, and (e) Ti–35Mo.

The micro-hardness of Ti–xMo and sintered Ti–xMo alloys (x = 25, 30, and 35 wt.%) was measured using an instrumented micro-indentation tester (THL370 Portable Hardness Tester, Germany) equipped with a Vickers diamond indenter. A load of 500 gf (HV0.5) was applied for 10 s at room temperature. Indentations were spaced at least three times the indent diagonal apart, and five measurements were averaged for each sample to ensure accuracy.

RESULTS AND DISCUSSION

Microstructural evolution

Field-emission scanning electron microscopy (FE-SEM) was performed on all samples before and after sintering at 1150 °C. Fig. 2 shows the FE-SEM images obtained for titanium nano-powder (TiNPs), molybdenum nano-powder (MoNPs), and titanium adding with varying proportions of molybdenum (25, 30, and 35 wt.%) before sintering at two different magnifications (5 µm and 2 µm). As shown in (Fig. 2a, b) the titanium and molybdenum powders exhibit nano-dimensional dimensions with distinct surface morphologies, which in turn affect their properties after the mixing and sintering processes. The images showed that titanium nanoparticles (TiNPs) have a semi-spherical shape with an average diameter of approximately 82 nm and are agglomerated in micro-scale clusters. These agglomerations are more pronounced at low magnification (2 µm), which is attributed to the high surface energy of the particles leading to the agglomeration of smaller secondary particles to form porous structures. Molybdenum nanoparticles (Mo NPs), on the other hand, display a surface character more akin to faceted particles, characterized by distinct inter-particle boundaries and an average diameter of around 76.7 nm. Additionally, the images revealed a more consistent particle size distribution when compared to titanium nanoparticles [32]. FE-SEM images of the pre-sintered pure Ti, Mo, and composite samples (Fig. 2c, d, and e) show the presence of a white layer on all samples. This observation indicates the formation of titanium and molybdenum oxide layers due to the exposure of the nano-powders to air.

This is consistent with the X-ray diffraction (XRD) results obtained, and clear agglomeration of the particles was observed at all percentages (25, 30, and 35 wt.%). This is attributed to the high surface strength of the nano powders. The average diameter of the mixed samples at the percentages (25, 30, and 35 wt.%) was found to be 81.16 nm, 88.26 nm, and 76.37 nm, respectively. Furthermore, agglomeration increases with increasing molybdenum powder content from 25 wt.% to 30 wt.%, and then decreases slightly at 35 wt.%, reflecting the effect of molybdenum nanoparticle (MoNPs) distribution on the microstructure. This is attributed to the differing surface properties of titanium and molybdenum, which influence dispersion when mixed with molybdenum powder. Additionally, the more uniform shape of molybdenum powder could play a role in preventing granule growth. [33].

FE-SEM images of the samples taken after sintering at 1150°C reveal that the titanium particles display a semi-spherical shape with an average diameter of 671 nm. This observed increase in diameter is due to granular growth and a decrease in surface energy during the sintering process. Moreover, the fact that the molybdenum powder is more uniform may have a contribution to the inhibition of the growth of the granules. [33].

FE-SEM images of the samples that were sintered at 1150°C indicate that the titanium particles have a semi-spherical shape with average diameter of 671 nm. This is because the observed growth in diameter is a result of granular growth and loss in surface energy through the sintering process. On another note, the surface oxide layers are important in determining the granular growth since they restrict inter-particle bonding as well as serving as a barrier to the process. [34].

After sintering the samples prepared using titanium powder and different concentrations of molybdenum powder (25, 30 and 35 wt.%) it was observed that the size of the nanoparticles had increased significantly after sintering than when they were pre-sintered. The difference in the particle size seemed to be directly affected by molybdenum powder proportion. The mean diameter of the sample particles of Ti-25Mo was around 923 nm. As the molybdenum concentration was however increased to Ti-30Mo, the diameter swelled to an average of 1110 nm but thereafter, it dropped to a considerable average diameter of about 574 nm. Also, following the sintering process, in all compositions, particles exhibited a more definite spherical shape with detail granular boundaries, unlike the unsintered models. Increase in grain size with molybdenum content

of 25 and 30 by weight is probably attributed to the enhanced atomic diffusion during the sintering procedure. Molybdenum has a relatively low surface energy and therefore, it enables the diffusion along the grain boundaries and thus, the fusion and growth of particles will be accelerated. Furthermore, the rise in the level of molybdenum can reduce the free energy of the particle surface and accelerate diffusion of growth nuclei and hence increase grain growth at higher temperatures [35]. This large decrease of average particle size at 35 wt.% is due to the saturation effect and the unique solubility of molybdenum in the titanium lattice. The effect encourages the creation of

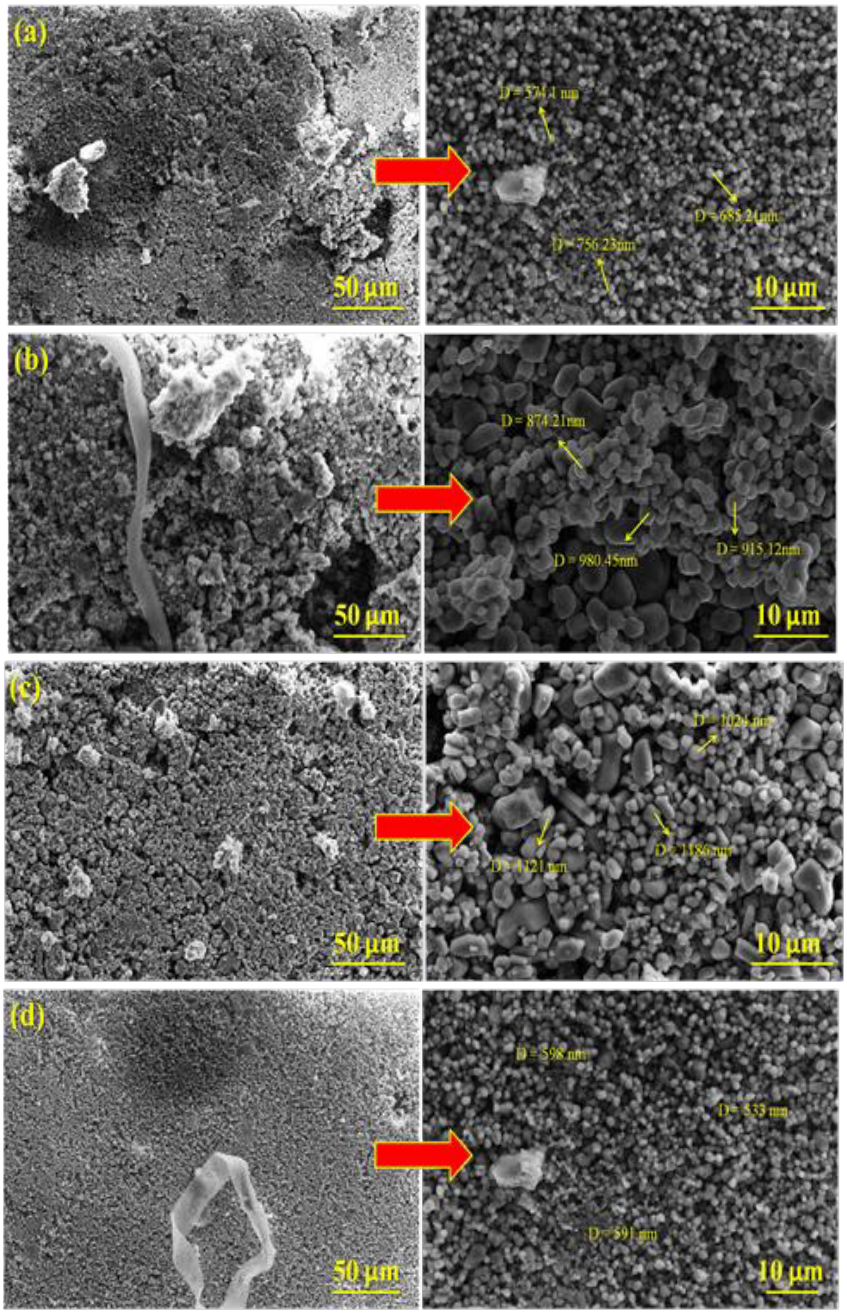

Fig. 3. FE-SEM micrographs of sintered samples at 1150 °C: (a) Ti nanoparticles, (b) Ti–25Mo, (c) Ti–30Mo, and (d) Ti–35Mo.

molybdenum-enriched areas or complex oxide (Ti-Mo-O), which impede the flow of the grain boundaries, consequently restricting the growth of the grains and leading to relatively small grains. This result correlates with the XRD result and supports the results of Li et al., who had previously found inhibited grain growth with molybdenum concentration exceeding its solubility level [36]. The semi-spherical shape of the powder particles after sintering indicates that the process occurred within the solid-state sintering range and that particle remodeling resulted from a reduction in surface energy via diffusion without melting. The more distinct particle boundaries in all samples indicate the completion of neck formation and the achievement of a high degree of internal density. Mechanically, particle growth at 25–30 wt.% leads to a decrease in yield strength, while reducing particle size at 35 wt.% improves hardness and toughness. Thus, increasing the molybdenum

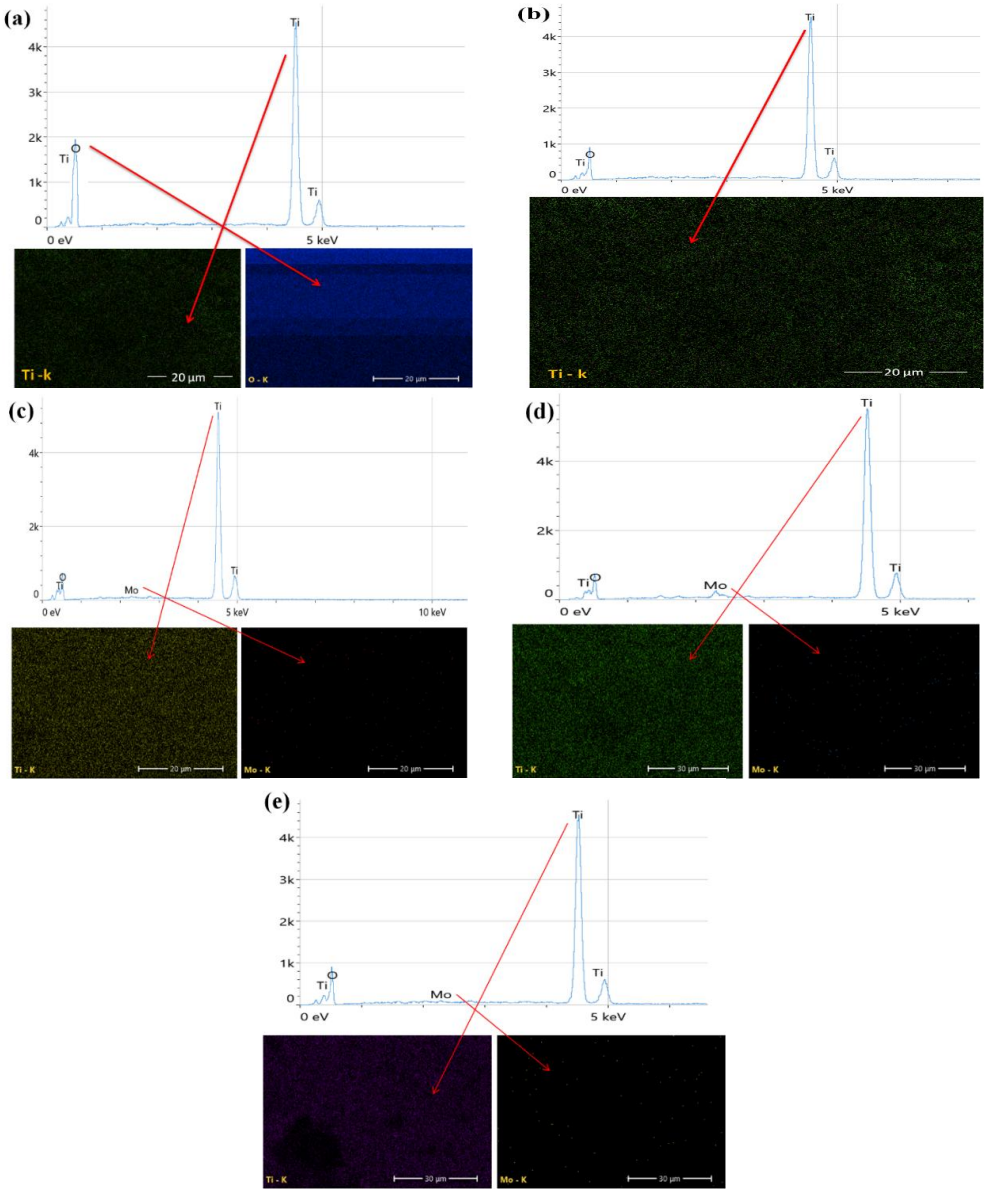

Fig. 4. EDX spectra of Ti nanoparticles before sintering (a) and sintered Ti and Ti–xMo samples (x = 25, 30, and 35 wt.%) at 1150 °C (b–e).

content promotes particle growth up to a certain point, after which a counterproductive effect occurs due to the formation of phases or oxides that stabilize the particle boundaries.

The EDX spectra (Fig. 4) confirmed the elemental composition of the prepared samples. For pure Ti samples, only Ti and O were detected before and after sintering, with a noticeable reduction in oxygen content after sintering. This is attributed to the inert atmosphere reduction during heat treatment, partial reduction of surface oxides, and increased density with reduced porosity. In Mo-containing samples, Ti, Mo, and O were identified, with Ti:Mo atomic ratios closely matching the nominal compositions (approximately 75:25, 70:30, and 65:35). These results are consistent with the XRD findings and indicate the absence of impurity phases in the prepared alloys.

XRD analysis of Ti-xMo powders

X-ray diffraction (XRD) was used to identify the crystalline phases and crystallite size of the prepared samples. The XRD pattern of molybdenum nano-powder (MoNPs) before sintering showed characteristic peaks at 2θ = 40.51°, 58.60°, and 73.66°, corresponding to the (110), (200), and (211) planes of cubic Mo with space group Im-3m (No. 229), lattice parameter a = 3.1472 Å, and angles α = β = γ = 90°, in agreement with JCPDS card No. 00-004-0809 Fig. 5a. After the addition of different Mo contents to titanium nano-powder (25, 30, and 35 wt.%) before sintering, the XRD patterns exhibited peaks at 2θ = 35.08°, 40.16°, and 62.93°, corresponding to the (100), (101), and (110) planes of hexagonal Ti with space group P63/mmc (No. 194), lattice parameters a = b = 2.9511 Å and c = 4.6843 Å, and angles α = β = 90° and γ = 120°, consistent with standard data (JCPDS 01-089-2762). The XRD pattern shows diffraction peaks at 2θ = 37°, 42.99°, and 62.43°, corresponding to the (101), (002), and (022) planes of cubic titanium oxide (TiO_2) with space group Fm-3m (No. 225), lattice parameter a = b = c = 4.2040 Å, and lattice angles α = β = γ = 90°, in excellent agreement with the standard JCPDS reference card (No. 98-005-6612). The characteristic diffraction

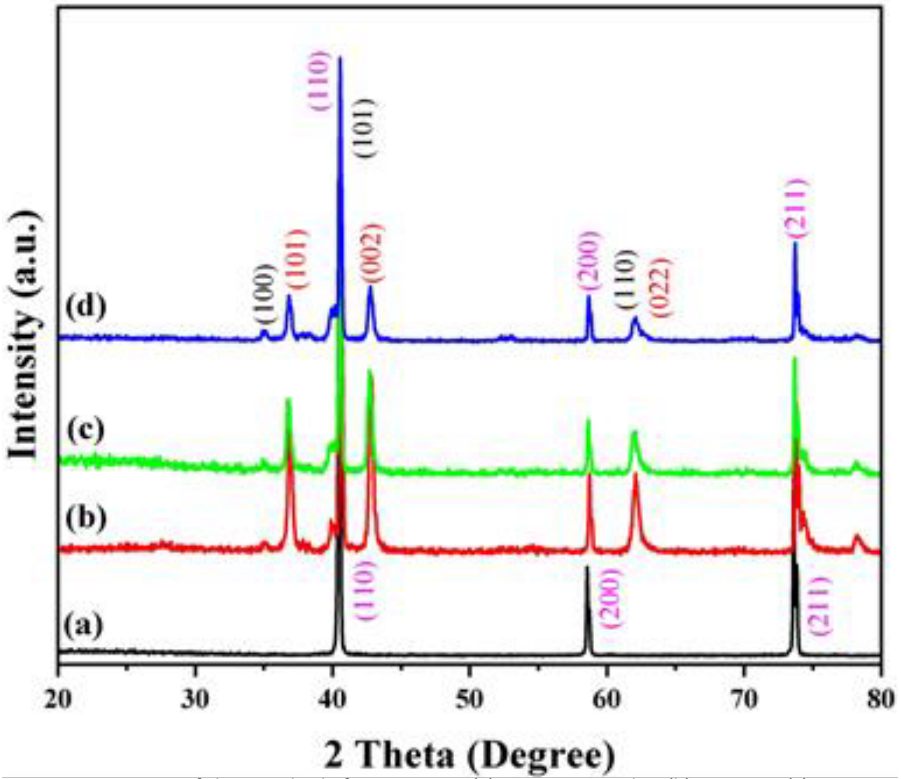

Fig. 5. XRD patterns of the samples before sintering: (a) Mo nanoparticles, (b) Ti–25Mo, (c) Ti–30Mo, and (d) Ti–35Mo.

peaks of molybdenum observed at 2θ = 40.51°, 58.60°, and 73.66° remained clearly visible after incorporation, as shown in Fig. 5b, c, and d). XRD results confirm the presence of individual metallic phases after blending, along with the formation of TiO_2, which is attributed to surface oxidation of titanium due to its high reactivity with oxygen, particularly in nano-powders with high surface-to-volume ratios. No additional peaks corresponding to impurities were detected before or after the blending process.

XRD analysis of sintered titanium powder revealed characteristic diffraction peaks at 2θ = 35.09°, 38.42°, 40.17°, 62.90°, 74.16°, and 77.37°, corresponding to the (100), (002), (101), (110), (200), and (201) planes of the hexagonal α-Ti (HCP) phase with space group $P6_3/mmc$, lattice parameters a = b = 2.9505 Å and c = 4.6826 Å, and angles α = β = 90° and γ = 120°, in good agreement with JCPDS No. 00-044-1294 (Fig. 6a). After sintering at 1150 °C, additional peaks at 2θ = 39.10°, 39.13°, and 56.51° were observed, corresponding to hexagonal Ti with space group P6/mm (No. 191), consistent with JCPDS No. 98-005-2521.

Moreover, diffraction peaks at 2θ = 36.07°, 41.24°, 44.05°, 54.32°, 62.75°, 64.05°, 69.01°, 69.79°, and 76.53° were indexed to the tetragonal rutile TiO_2 phase (space group $P4_2/mnm$, No. 136), with lattice parameters a = b = 4.5930 Å and c = 2.9590 Å, matching JCPDS No. 98-900-4142 (Fig. 6b).

Upon the addition of Mo nano-powder (25, 30, and 35 wt.%) to Ti nano-powder and sintering at 1150 °C, new diffraction peaks appeared (Fig. 6c, d, and e), indicating phase evolution. Peaks at 2θ = 26.71°, 38.13°, 42.88°, 53.70°, 55.03°, 62.19°, and 67.75° correspond to the tetragonal $TiMoO_2$ phase (space group $P4_2/mnm$, No. 136), with lattice parameters a = b = 4.7160 Å and c = 2.8990 Å, in agreement with JCPDS No. 98-010-9173. Additionally, retained peaks at 2θ = 35.09°, 40.17°, 62.96°, and 76.21° confirm the persistence of the hexagonal Ti phase ($P6_3/mmc$, No. 194),

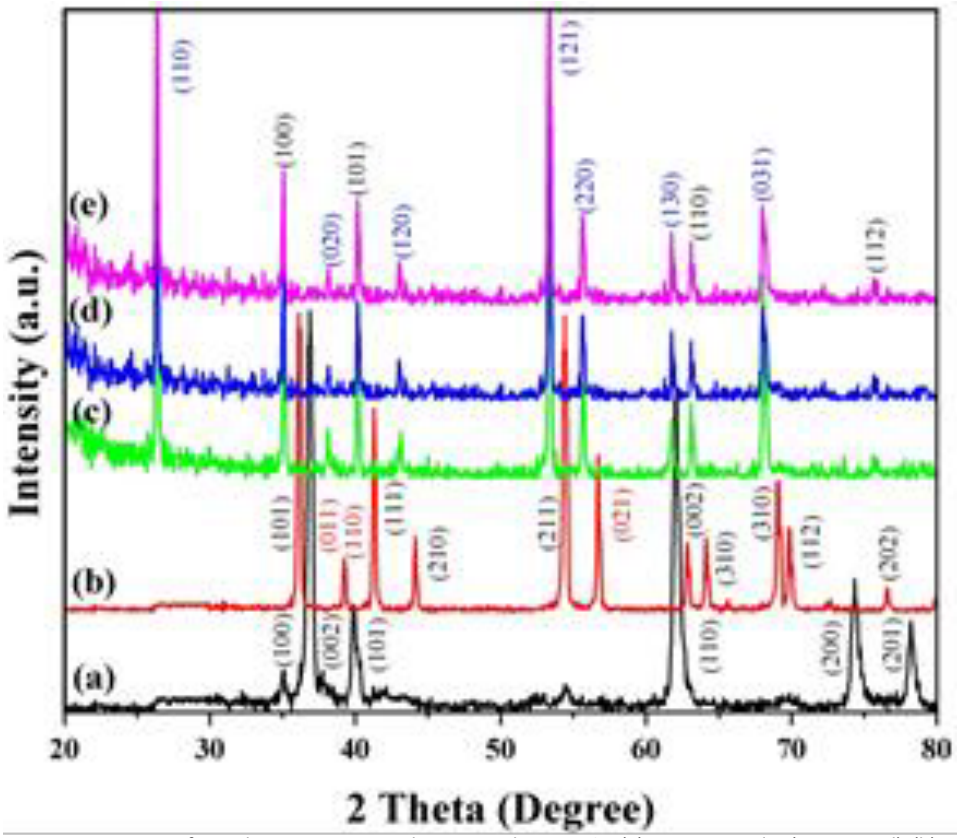

Fig. 6. XRD patterns of Ti and Ti–xMo nanopowders sintered at 1150 °C: (a) Ti nanoparticles (un-sintered), (b) Ti nanoparticles, (c) Ti–25Mo, (d) Ti–30Mo, and (e) Ti–35Mo.

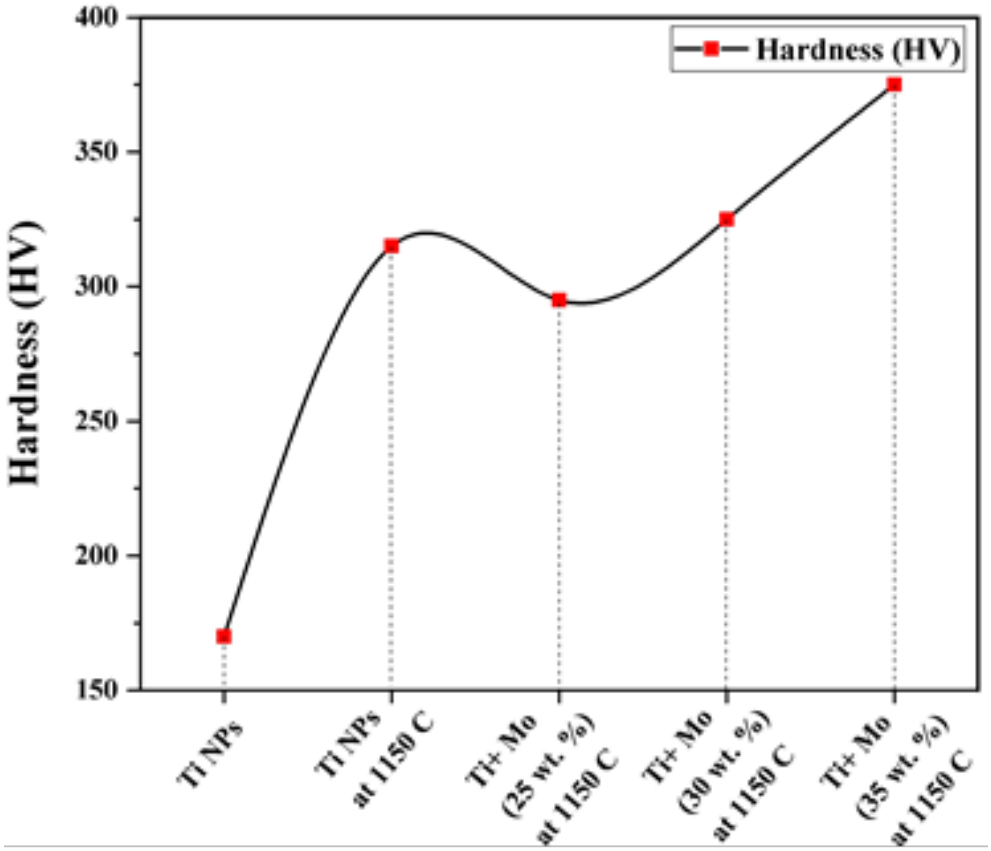

Fig. 7. Shows values of Vickers hardness obtained on the prepared samples under various processing conditions.

consistent with JCPDS No. 01-089-4893.

XRD results indicate that sintering of mixed Ti and Mo nano-powders led to structural overlap and the formation of a TiO_2–MoO_2 phase, evidenced by the appearance of new characteristic peaks, while the pure Ti phase remained detectable. The oxide formation is attributed to pre-existing surface oxides on Ti and Mo nanoparticles and/or moisture-derived oxygen, with enhanced atomic mobility at elevated temperatures promoting solid-state diffusion and chemical interaction [37]. No impurity-related diffraction peaks were observed after sintering.

Mechanical properties

Hardness testing is a key parameter for assessing the mechanical behavior of materials after processing steps such as sintering and alloying [38]. Vickers hardness of pressed sample of titanium nano-powder in the un-sintered form, following sintering at 1150°C and addition of molybdenum nano-powder at levels of 25, 30 and 35 wt.% were tested in this work. Fig. 7 revealed that sintering had a great effect on the hardness of the titanium nanopowder, increasing the HV 170 in green compact titanium nanopowder, which was sintered at 1150°C, to HV 315. This is mainly due to the fact that there was a higher degree of densification and lower porosity because of a rearrangement of the grains and diffusion bonding that brought about a higher level of structural cohesion and microstructural stability. Also, sintering created additional crystal formation, which reinforced the material [39]. But when 25 wt.% molybdenum was added, the hardness (HV 295) decreased a little relative to sintered pure titanium, which can be explained by the fact that the b-phase was not evenly distributed or formed coarse grains [40]. Another important observation was at increased levels of molybdenum addition (30 and 35 wt.%), the hardness increased significantly with values of 325 and 375 being

obtained under HV and HV respectively. This is mainly attributed to solid-solution strengthening that is occasioned by the addition of molybdenum atoms into the titanium lattice. This mechanism increases distortion of lattices and prevents the motion of dislocations. Additionally, grains interconnected with greater levels of molybdenum can be stabilized in a secondary solid state, and grains are refined which also increases crystal slip resistance within the microstructure. [41,42]. In general, these findings can be used to conclude that the sintering technique and the controlled introduction of molybdenum nano-powder have a high impact in increasing the hardness of titanium alloys.

The results have shown that sintering at 1150°C is the key factor of enhancing the hardness and other mechanical characteristics of nano-titanium alloys. The main method through which this improvement is obtained is by decreasing porosity and enhancing intergranular bonds [43, 44]. Also, 30 to 35 wt.% of molybdenum was added which leads to the maximum hardness levels, due to the actions such as solid-solution strengthening, solid phase stabilization, and grain refinement. As a result, it is essential to have a fine control of the sintering conditions as well as the content of molybdenum to maximize the hardness and life of nano-titanium powder systems [45, 46, 47].

CONCLUSION

It was a comprehensive study on the effect of the sintering process on the microstructure, chemical composition and mechanical properties of Titanium-Molybdenum alloys. The analysis of the Field-Emission Scanning Electron Microscopy (FE-SEM) showed distinct powder morphologies and composition-dependent agglomeration behavior before sintering, and tremendous growth of the grain after sintering at 1150°C. Microstructural changes showed that there is lessening of the voids and an increase in interparticle bonding, which are essential considerations of ensuring substantial enhancement in the mechanical properties of the Molybdenum-reinforced titanium nanoalloys. The EDX and XRD analysis showed the considerable increase in the chemical purity and stability of the phase after sintering, which was mainly explained by the application of protective argon atmosphere, which effectively eliminated oxidation. Also, the sintering process resulted in significant hardening of pure titanium. Even though the addition of molybdenum led to the slight decline in hardness, as more of it was added, the mechanical properties increased. This emphasizes the high significance of establishing optimum levels of molybdenum and right conditions of sintering during plan design of titanium-molybdenum alloys. Under sintering at 1150°C and alloying with Mo, the hardness of nano-titanium improved significantly as the hardness of pure Ti of 170 HV declined to 375 HV of a Ti-35 wt.% Mo alloy. This high increase in hardness is mainly due to solid solution strengthening, refinement of grains and development of stable molybdenum rich phases that hinder the movement of the dislocations.

CONFLICT OF INTEREST

The authors declare that there is no conflict of interests regarding the publication of this manuscript.

REFERENCES

1. Lütjering G, Albrecht J, Sauer C, Krull T. The influence of soft, precipitate-free zones at grain boundaries in Ti and Al alloys on their fatigue and fracture behavior. Materials Science and Engineering: A. 2007;468-470:201-209.
2. Isakdjanov RR. Theoretical Bases of Studying the Gnoseology of Central Asian Philosophy. Theoretical and Applied Science. 2019;75(07):22-25.
3. Bannon BP, Mild EE. Titanium Alloys for Biomaterial Application: An Overview. Titanium Alloys in Surgical Implants: ASTM International100 Barr Harbor Drive, PO Box C700, West Conshohocken, PA 19428-2959; 1983. p. 7-15.
4. Niinomi M, Boehlert CJ. Titanium Alloys for Biomedical Applications. Springer Series in Biomaterials Science and Engineering: Springer Berlin Heidelberg; 2015. p. 179-213. http://dx.doi.org/10.1007/978-3-662-46836-4_8
5. Titanium and Titanium Alloys: Wiley; 2003.
6. Whittaker D, Froes FH. Future prospects for titanium powder metallurgy markets. Titanium Powder Metallurgy: Elsevier; 2015. p. 579-600.
7. Anurag, kumar R, Roy S, Joshi KK, Sahoo AK, Das RK. Machining of Ti-6Al-4V ELI Alloy: A brief review. IOP Conference Series: Materials Science and Engineering. 2018;390:012112.
8. Sidhu SS, Singh H, Gepreel MA-H. A review on alloy design, biological response, and strengthening of β-titanium alloys as biomaterials. Materials Science and Engineering: C. 2021;121:111661.
9. Lütjering G, Williams JC. Titanium. Engineering Materials and Processes: Springer Berlin Heidelberg; 2003.
10. Huang S, Zhao Q, Wu C, Lin C, Zhao Y, Jia W, et al. Effects of β-stabilizer elements on microstructure formation and mechanical properties of titanium alloys. J Alloys Compd. 2021;876:160085.
11. Properties and Selection: Nonferrous Alloys and Special-Purpose Materials: ASM International; 1990.
12. Huzum B, Puha B, Necoara R, Gheorghevici S, Puha G, Filip A, et al. Biocompatibility assessment of biomaterials used in orthopedic devices: An overview (Review). Exp Ther Med. 2021;22(5).
13. Shankar S, Nithyaprakash R, Abbas G. Tribological Study on Titanium Based Composite Materials in Biomedical Applications. Composites Science and Technology: Springer Singa-

pore; 2020. p. 215-241.
14. Hybasek V, Fojt J, Malek J, Jablonska E, Pruchova E, Joska L, et al. Mechanical properties, corrosion behaviour and biocompatibility of TiNbTaSn for dentistry. Materials Research Express. 2020;7(1):015403.
15. Dahmani M, Fellah M, Hezil N, Benoudia M-C, Abdul Samad M, Alburaikan A, et al. Structural and mechanical evaluation of a new Ti-Nb-Mo alloy produced by high-energy ball milling with variable milling time for biomedical applications. The International Journal of Advanced Manufacturing Technology. 2023;129(11-12):4971-4991.
16. Niinomi M, Nakai M. Ti-Based Biomedical Alloys. Novel Structured Metallic and Inorganic Materials: Springer Singapore; 2019. p. 61-76.
17. Chui P, Jing R, Zhang F, Li J, Feng T. Mechanical properties and corrosion behavior of β-type Ti-Zr-Nb-Mo alloys for biomedical application. J Alloys Compd. 2020;842:155693.
18. Savio D, Bagno A. When the Total Hip Replacement Fails: A Review on the Stress-Shielding Effect. Processes. 2022;10(3):612.
19. Hamadi F, Fellah M, Hezil N, Bouras D, Laouini SE, montagne A, et al. Effect of milling time on structural, physical and tribological behavior of a newly developed Ti-Nb-Zr alloy for biomedical applications. Adv Powder Technol. 2024;35(1):104306.
20. Liu F, Zhang Z, Zhang L, Meng RN, Gao J, Jin M, et al. Effect of metal ions on Alzheimer's disease. Brain and Behavior. 2022;12(3).
21. Campos-Quirós A, Cubero-Sesín JM, Edalati K. Synthesis of nanostructured biomaterials by high-pressure torsion: Effect of niobium content on microstructure and mechanical properties of Ti-Nb alloys. Materials Science and Engineering: A. 2020;795:139972.
22. Xu W, Tian J, Liu Z, Lu X, Hayat MD, Yan Y, et al. Novel porous $Ti_{35}Zr_{28}Nb$ scaffolds fabricated by powder metallurgy with excellent osteointegration ability for bone-tissue engineering applications. Materials Science and Engineering: C. 2019;105:110015.
23. Moshokoa NA, Phasha M, Raganya L, Makoana NW, Mkhonto D, Makhatha ME. Tensile Properties of Quenched Binary Ti-Mo Alloys for Potential Use as Orthopedic Implants. Springer Proceedings in Physics: Springer Nature Singapore; 2025. p. 302-313.
24. Li H, Cai Q, Li S, Xu H. Effects of Mo equivalent on the phase constituent, microstructure and compressive mechanical properties of Ti–Nb–Mo–Ta alloys prepared by powder metallurgy. Journal of Materials Research and Technology. 2022;16:588-598.
25. Ho WF, Ju CP, Chern Lin JH. Structure and properties of cast binary Ti–Mo alloys. Biomaterials. 1999;20(22):2115-2122.
26. Kobayashi S, Okano S. The effects of oxygen addition on microstructure and mechanical properties of Ti-Mo alloys for biomedical application. Frontiers in Bioengineering and Biotechnology. 2024;12.
27. Shahryari E, Poletti MC, Pierer S, Preisler D, Harcuba P, Stráský J, et al. Strengthening effect of Mo in biocompatible titanium alloys. Materials Science and Engineering: A. 2025;948:149328.
28. Huang J, Bahador A, Kondoh K. Microstructure development and strengthening behaviour in hot-extruded Ti-Mo alloys with exceptional strength-ductility balance. J Alloys Compd. 2025;1010:177195.
29. Toualbia K, Fellah M, Hezil N, Milles H, Djafia Z. Effect of milling time on structural, mechanical and tribological properties of nanostructured HIPed near type Ti-15Mo alloys. Tribology International. 2024;197:109731.
30. Awad AH, Saood M, Aly HA, Abdelghany AW. Role of Mo and Zr Additions in Enhancing the Behavior of New Ti–Mo Alloys for Implant Materials. Metals and Materials International. 2024;31(5):1232-1253.
31. Gao K, Zhang Y, Yi J, Dong F, Chen P. Overview of Surface Modification Techniques for Titanium Alloys in Modern Material Science: A Comprehensive Analysis. Coatings. 2024;14(1):148.
32. Jisen Y, Minghui W, Tingan Z, Fang X, Xi Z, Ke Z, et al. Research progress in preparation technology of micro and nano titanium alloy powder. Nanotechnology Reviews. 2024;13(1).
33. Xin F, Ding W, Tao Q, Tian H, Chen G, Qin M, et al. Effect and Evolution of Oxide Film in the HDH-Ti Powder Surface on Densification Behavior During Sintering. Metallurgical and Materials Transactions A. 2022;53(4):1164-1175.
34. Hwang H-W, Park J-H, Lee D-G. Effect of Molybdenum Content on Microstructure and Mechanical Properties of Ti-Mo-Fe Alloys by Powder Metallurgy. Applied Sciences. 2022;12(14):7257.
35. Preparation of titanium-iron hydrogen storage alloy in microgravity. Metal Powder Report. 1999;54(1):35.
36. Li Z-B, Zhang G-H, Chou K-C. Synergistic effects of multi-strengthening mechanisms in exceptionally high-strength W-Ni-Fe composites. J Alloys Compd. 2023;969:172361.
37. Han R, Bao Z, Zhu Y, Li N, Tang M, Zhang H, et al. High Temperature Oxidation Resistance Performance of TiC/Mo Composite by Spark Plasma Sintering. Mater Sci. 2022;28(2):171-177.
38. Wright WW. Materials science and engineering. An introduction 2nd Edition W. D. Callister, Jr John Wiley and Sons, New York, 1991. pp. xxi + 791, price E53.00. ISBN 0-471-50488-2. Polym Int. 1993;30(2):282-283.
39. Ram RK, Pandey SM. Microstructural and Mechanical Properties of Tungsten-Inert-Gas-Clad TiB2/Mo/Cr Composite Coating on AISI 304 Stainless Steel. J Mater Eng Perform. 2024;34(14):13898-13913.
40. Liang SX, Liu KY, Shi YD, Yin RS, Dong LH, Zhang XY, et al. Strength-toughness synergic Ti-Mo double harmonic alloys prepared via powder metallurgy. Mater Lett. 2024;355:135445.
41. Akhlaghi M, Körner C. Comparison between nitriding behavior of Mo-Ti and Mo-V alloys. Int J Refract Met Hard Mater. 2023;112:106126.
42. Awad AH, Aly HA, Saood M. Physical, mechanical, and corrosion properties of Ti–12Mo and Ti–15Mo alloys fabricated by elemental blend and mechanical alloying techniques. Materials Chemistry and Physics. 2024;312:128661.
43. Balan AE, Al-Sharea A, Lavasani EJ, Tanasa E, Voinea S, Dobrica B, et al. Paraffin-Multilayer Graphene Composite for Thermal Management in Electronics. Materials. 2023;16(6):2310.
44. Ayoub RH, Al-Timimi MH, Abdullah MZ. Enhancements of Structural and Optical Properties of MgO: SnO_2 Nanostructure Films. East European Journal of Physics. 2023(3):546-554.
45. Ahmed NS, Abduljabbar HM. A Study of the Land Cover of Razzaza Lake during the Past 25 Years Using Remote Sensing Methods. Ibn AL-Haitham Journal for Pure and Applied Sciences. 2023;36(1):158-169.
46. Remediation of Olive Mill Industry Wastewater with Titanium Dioxide (TiO_2), Silisium Dioxide (SiO_2) and Zinc Oxide (ZnO) Using Ultrasound. Advance in Environmental Waste Management and Recycling. 2021;4(2).
47. Ahmed G, Ahmed G. Coclosed Rickart Modules. Ibn AL-Haitham Journal For Pure and Applied Sciences. 2018:452-462.